Spatial Scale Transformation-based Estimation Model for Fresh Grass Yield: A Case Study of the Xilingol Grassland, Inner Mongolia, China

Haixin Liu (gislhx@hebeu.edu.cn)
Hebei University of Engineering https://orcid.org/0000-0001-5117-3241
Anbing Zhang (zhanganbing@hebeu.edu.cn)
Hebei University of Engineering
Yuling Zhao
Hebei University of Engineering
Anzhou Zhao
Hebei University of Engineering
Dongli Wang
Hebei University of Engineering

Research Article

Keywords: Remote sensing, MODIS, Vegetation coverage, spatial scale transformation (SST), fresh grass yield (FGY)

Posted Date: March 9th, 2021

DOI: https://doi.org/10.21203/rs.3.rs-182923/v1

Spatial Scale Transformation-based Estimation Model for Fresh Grass Yield: A Case Study of the Xilingol Grassland, Inner Mongolia, China

Haixin Liu [1,2,*], Anbing Zhang [1,2*], Yuling Zhao [1,2], Anzhou Zhao[1] and Dongli Wang [1]

[1] College of Mining and Geomatics, Hebei University of Engineering, Handan 056038, China;

[2] Heibei Collaborative Innovation Center of the Comprehensive Development and Utilization of Coal Resource, Hebei University of Engineering, Handan 056038, Hebei, China

Corresponding author:

Haixin Liu

Email: gislhx@hebeu.edu.cn

Tel: +860310 3967616

Fax: +860310 3968766

Anbing Zhang

Email: zhanganbing@hebeu.edu.cn

Tel: +860310 3969519

Fax: +860310 3969519

Abstract: Estimating the grass yield of a grassland is of vital theoretical and practical significance for reasonably determining its grazing capacity and maintaining its ecological balance. On that account, this paper first compares model precision by adopting normalized differential vegetation index (NDVI) and net primary productivity (NPP) as grass yield estimation factors, and then proposes a spatial scale transformation (SST)-based estimation model for fresh grass yield (FGY) adopting NPP as its estimation factor. Next, it takes the grassland in Xilingol League, Inner Mongolia as the study area for precision verification and grass yield estimation. Results indicated that: (1) The precision of the model adopting NPP as the estimation factor was clearly higher than that of the model adopting NDVI. (2) Through modifying NPP, the SST-based FGY estimation model could greatly improve estimation precision. The relative precisions of the estimation models constructed using linear and power functions were 18.16% and 18.35%, respectively. (3) The estimation models constructed using linear and power functions were employed to estimate the grass yield of the grassland in Xilingol League, and the total FGYs estimated by them were 8.777×10^{10} kg and 8.583×10^{10} kg, respectively. The two models obtained roughly the same estimates, but there were significant differences between them in the spatial distributions of FGY per unit.

Keywords: Remote sensing; MODIS; Vegetation coverage; spatial scale transformation (SST); fresh grass yield (FGY)

1. Introduction

The grassland ecosystem is one of the most widely distributed ecosystems around the world, covering about 40% of land surface (Suttie et al., 2005). So far, there are approximately 400 million hectares of natural grasslands in China. Mainly distributed in the Inner Mongolia Autonomous Region (Inner Mongolia for short), the Xinjiang Uygur Autonomous Region (Xinjiang for short), and Sichuan Province, they account for 41.7% of China's total land area, and constitute the largest terrestrial ecosystem in China(Xie et al., 2001; Xu et al., 2013). Grasslands not only produce feed for animal husbandry, but also fulfill many important ecological service functions, such as carbon fixation and oxygen release, wind break provision and sand fixation, headwater conservation, soil and water conservation, and biodiversity maintenance (Fry et al., 2013).The grass yield of grasslands is both the material basis of grassland ecosystem maintenance and the most direct reflection of grassland status (Xu and Yang, 2009), and it determines the strength of the functions of the grassland ecosystem. Thus, to timely and accurately identify the spatio-temporal distribution of grassland grass yield and grasp its interannual dynamic variation provides an essential scientific basis for determining grazing capacity with reasonable certainty, and has vital theoretical and practical significances for keeping grassland ecological balance and arranging livestock production.

The grass yield of a grassland directly reflects its productivity. The traditional methods of assessing grassland productivity mainly include ground surveys, statistical models (Gao et al., 2009; Li et al., 2003; Liu et al., 2007; Yang et al., 2008), process models (Feng and Zhao, 2011; Goetz et al., 1999; Luo et al., 2012), and parameter models (Li et al., 2007; Zhang et al., 2008). The development of remote sensing technology has driven the emergence of numerous studies using this technology to estimate the productivity and grass yield of grasslands, and a series of remote sensing estimation models have been put forward(Liu et al., 2020). This technology, when used to estimate the grass yield of grasslands, saves both time and labor, and offers efficient decision-making in grassland management from a macroscopic perspective.

Literature in this field has shown that grass yield is closely related to vegetation indices. Aided by all kinds of vegetation indices, scholars have introduced linear functions, power

functions, and other mathematical relationships to construct remote sensing estimation models for grass yield (Bella et al., 2004; Gao et al., 2013; Xu et al., 2007; Yang et al., 2007). For instance, Gao et al. (Gao et al., 2013) investigated the spatial distribution of aboveground and underground biomass in the Xilingol Grassland, Inner Mongolia using MODIS NDVI. Xu et al. (Xu et al., 2008) presented a systematic model that could be used to estimate the grass yield of grasslands on mainland China based on MODIS NDVI and ground samples. Yang et al. (Yang et al., 2009) estimated the aboveground biomass in Tibet using the MODIS enhanced vegetation index (EVI), and analyzed the relationship between aboveground biomass on grasslands and meteorological factors. However, as far as the suitability of a vegetation index to a specific region or environment is concerned, further discussion and experiments are still needed. Some studies hold that NDVI enjoys some advantages when it comes to the remote sensing estimation of grass yield (Ni, 2004). However, the instability and supersaturation of NDVI under different vegetation coverages tend to introduce indeterminate errors into grass yield estimation. In recent years, many scholars have attempted to estimate grass yield with other remote sensing derivative products (such as GPP and MODIS PSNnet). For example, Fu et al. (Fu et al., 2014)combined MODIS GPP and NDVI with calculated vegetation coverage and actual survey data to estimate the grass yield of grasslands in Sichuan Province. Zhao et al. (Zhao et al., 2014) directly constructed a regression model based on MODIS PSNnet and ground survey data, and used it to estimate the grass yield of the Xilingol Grassland.

In addition, as far as remote sensing estimation models for grass yield are concerned, there is also the frequent problem of inconsistency between ground sample data and digital remote sensing images on spatial scales. The main reason is because, on the one hand, sample collection usually adopts a quadrat size of 1 m2 for the sake of grassland protection. On the other, remote sensing data adopted for large-scale grass yield estimation often have a spatial resolution of 30-1,000 m, and the surface features within each pixel are not singular; the spectral information contained has integrated the spectral characteristics of different vegetation types within different pixels (Zribi et al., 2003). Thus, for the purpose of improving the precision of estimation models, the spatial scale transformation (SST) of remote sensing images and ground samples is highly necessary.

In sum, studies on the estimation of grass yield using remote sensing technology have achieved numerous significant practical results, however, in-depth research is still needed to solve a series of problems:

① There are still controversies around the suitability of various vegetation indices to different environments and the precision of grass yield estimates based on them. In particular, net primary productivity (NPP) is defined as the residual primary productivity of the total organic matter content produced by a green plant within a unit time and unit area after deducting the proportion consumed by the plant itself for autotrophic respiration (Zhou et al., 2020). It is worth exploring whether annual NPP can be adopted as the primary factor for grass yield estimation.

② How to solve the problem regarding the effect of the inconsistency between ground samples and remote sensing data on spatial scales on the precision of the remote sensing estimation model for grass yield?

This paper first draws a comparison between NDVI and NPP as grass yield estimation factors, and then proposes the SST for ground samples and remote sensing data based on vegetation coverage on different spatial scales, thus constructing a new remote sensing estimation model for grass yield. Next, it verifies the model using measured ground samples, and performs grass yield estimation for the study area on this basis.

·2. Study Area

The area adopted for study in this paper is the Xilingol Grassland, a typical temperate grassland located in central Inner Mongolia, northern China (41°35′~46°46′ in north latitude, and 111°09′~119°58′ in east longitude, as shown in Figure 1). It occupies a total area of 202,580 km^2, 192,512 km^2 (95.03%) of which is grassland. The dominant grassland type is natural grassland, which accounts for 97.2% of total grassland area. The study area has the climatic characteristics of a typical temperate continental semi-arid climate zone, and is cold in the winter and hot in the summer, with mean annual temperatures of 1.3~4.8℃ and mean annual precipitation of 150~400 mm. Precipitation increases progressively from west to east, and the annual precipitation distribution is uneven (70% concentrated in the period from June to August), with significant interannual variability.

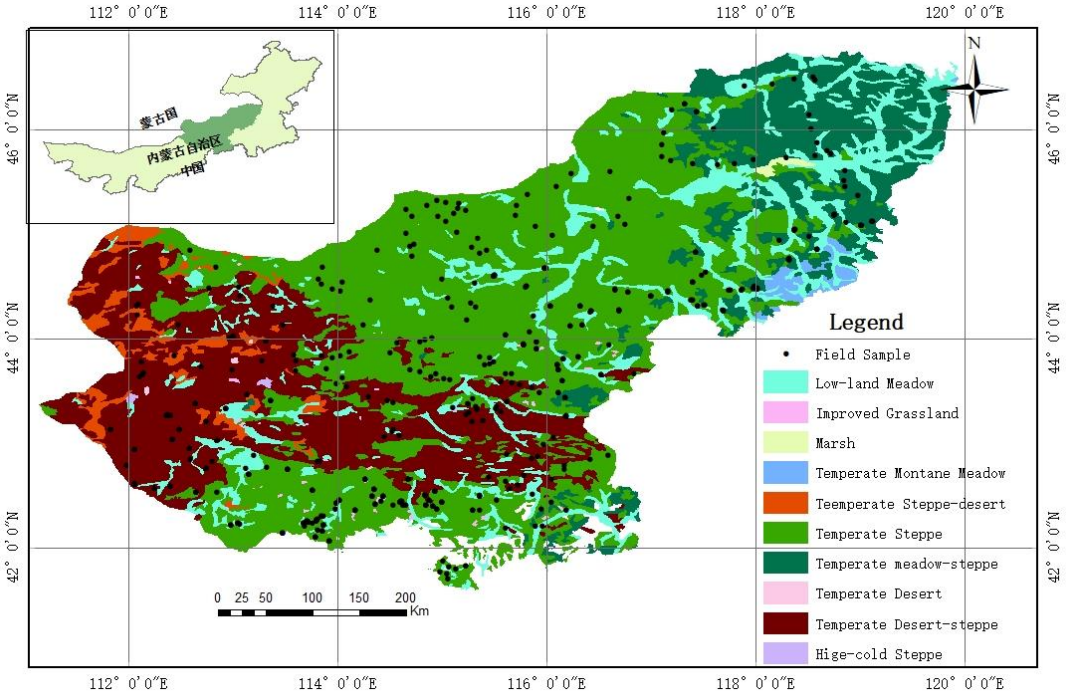

Figure 1. Grassland types and sampling points in the study area.

3. Data and Processing

3.1 Ground survey data

The ground sample data adopted in this paper were measured ground quadrat data collected by the local grassland authority as entrusted by the Grassland Supervision and Monitoring Center of the Chinese Ministry of Agriculture during July-August (flourishing period for grass), 2013. Fig. 1 shows the spatial distribution of quadrats (1 m × 1 m in size). The main sample variables included quadrat longitude and latitude, grassland type, altitude, vegetation type, FGY, measured vegetation coverage (MVC), community height, grazing intensity, and sampling time. The FGY for samples was determined by mowing all the plants within quadrats to ground level and weighing them. Considering that ground sample data quality can substantially affect the estimation precision of models (Matsushita and Tamura, 2002), ground sample data were put through rigorous testing and standardized screening before modeling. After rejecting individual abnormal data based on grassland type and multi-year mean quadrat status, this study ultimately selected a total of 460 sample data (400 randomly selected for modeling, and 60 for precision verification). The quantities and sites of the samples used for modeling and precision verification represented the main grassland types and grass yield in this area.

3.2 Remote sensing data

The remote sensing data adopted in this paper were mainly derived from the MOD13A1-NDVI and MOD17A3-NPP data products from the official website of the National Aeronautics and Space Administration (NASA). MOD13A is a 16-day synthetic product, with a spatial resolution of 500 m. To effectively eliminate the errors caused by cloud cover, solar zenith angle, and atmosphere and to improve the quality of images (Liu et al., 2016), the NDVI data in the vegetation growth period of the study area (from April 1 to October 31, 2013) were preprocessed using the maximum value composite method (Formula (1)), and marked as ANDVI. MOD17A3-NPP is an annual product, with the same spatial resolution of 500 m and marked as ANPP.

$$ANDVI = MAX(NDVI_i) \tag{1}$$

where $ANDVI$ is the annual maximum value of NDVI; $NDVI_i$ is the NDVI data from each stage in the study period.

4. Research Methods

4.1 Estimation and modification of vegetation coverage

(1) Estimation of vegetation coverage

It is assumed that each pixel of the study area consists of two parts: that with vegetation coverage and that without (bare land), and the spectral information acquired by remote sensors is a linear combination of two pure components after weighting based on the area ratio. On this basis, the current classical binary pixel method (Ge et al., 2018) is adopted to calculate vegetation coverage from Formula (2) based on ANDVI data. The result is marked as AVC.

$$AVC_i = \frac{ANDVI_i - ANDVI_{\min}}{ANDVI_{\max} - ANDVI_{\min}} \tag{2}$$

Where i is geographical position; AVC is estimated vegetation coverage; $ANDVI$ is the annual maximum value of NDVI; $ANDVI_{max}$ is the maximum ANDVI of the study area; $ANDVI_{min}$ is the minimum ANDVI. This paper adopts the ANDVI value corresponding to a cumulative frequency of 95% as $ANDVI_{max}$, and that corresponding to a cumulative frequency of 5% as $ANDVI_{min}$.

(2) Modification of vegetation coverage

MVC is usually performed with discrete points based on the design scheme, while subsequent grass yield estimation is conducted pixel by pixel. Assuming that the vegetation coverage of the pixel where a sample is located is uniform and consistent with the measured vegetation coverage of the sample, to obtain the measured vegetation coverage of the entire study area, this paper proposes to modify AVC using MVC, as described below:

① Exact AVC based on the position of the quadrat, and perform margin calculation between MVC and AVC to obtain residual α (Formula (3)).

$$\alpha = MVC - AVC \tag{3}$$

② Provide Kriging interpolation for the calculated residual, modify AVC using image operation (Formula (4)), and mark it as RAVC.

$$RAVC = AVC + \alpha \tag{4}$$

4.2 Modification of NPP

Some studies have pointed out that the vegetation index (VI) is highly correlated with light use efficiency (LUE) and fraction of photosynthetically active radiation (FPAR) (Inoue et al., 2008; Viña and Gitelson, 2005). Related literature has confirmed that VI is a reliable reflection of LUE and FPAR, and that there is a high correlation between GPP/NPP and VI^2 × PAR (photosynthetically active radiation) (Gitelson et al., 2012; Wu et al., 2010). Based on the above parameter relationships, this paper introduces ANPP_NDVI (Formula (5)) to express ANPP modified according to the above principle.

$$ANPP_{\mathrm{NDVI}} = ANPP \times ANDVI^2 \tag{5}$$

4.3 SST of grass yield data

According to a comparison between FGY and ANPP, FGY comes from measured ground samples, with a spatial scale of 1 m, while ANPP is the MOD17A3-NPP data product with a spatial resolution of 500 m. For this reason, directly adopting ANPP for FGY estimation introduces unknown factors due to the inconsistency between spatial scales and lowers the fitting precision of the model.

Similarly, a comparison between AVC and RAVC reveals that AVC is calculated using ANDVI according to the binary pixel method, with a spatial scale of 500 m, whereas RAVC assumes that the vegetation coverage of each pixel is uniform and consistent with the measured

vegetation coverage of the sample. RAVC can be regarded by default as the vegetation coverage of the sample, with a spatial scale of 1 m. Assuming the coefficient of SST between them as *k*, the value of *k* can be calculated from the ratio of AVC to RAVC.

Assuming that there is a proportional relationship between FGY and vegetation coverage, the coefficient of SST can also be regarded as the ratio of the grass yield per unit with a spatial scale of 500 m (FGY_{500}) to the grass yield per unit with a ground measured spatial scale of 1 m (FGY) (Formula (6)).

$$\frac{AVC}{RAVC} = k = \frac{AFY_{500}}{AFY} \tag{6}$$

As can be seen from the above assumptions and analysis, the SST between FGY500 and FGY can be calculated based on AVC and RAVC.

4.4 Precision verification

To verify the precision of different remote sensing estimation models for FGY, this paper selects the commonly-used relative estimation error (REE) for precision evaluation. The formula is given below:

$$REE = \sqrt{\frac{\sum[(y_i - y_i^{'}) / y_i^{'}]^2}{N}} \tag{7}$$

where y_i is the survey data; *yi'* is the estimate from the regression model; *N* is the number of validation points.

To evaluate the total FGYs estimated by different models, this paper adopts relative estimation precision for quantitative analysis according to the following formula:

$$RSP_{ij} = 1 - \frac{\vartheta_{si} - \vartheta_{sj}}{\vartheta_{si}} \tag{8}$$

where RSP_{ij} is the estimation precision of model *j* relative to model *i*; ϑ_{si} is the total FGY of the entire study area estimated by model *i*; ϑ_{sj} is FGY estimated by model *j*.

5. Results and Discussion

5.1 Comparison of ANDVI and ANPP as grass yield estimation factors

As pointed out by related literature, in the remote sensing estimation of grass yield, NDVI produces desirable results as an estimation factor (Liu et al., 2020); however, due to its

supersaturation, it tends to underestimate grass yield in high-yield regions. In view of this problem, this paper proposes to adopt NPP, instead of NDVI, as the primary factor for grass yield estimation. Meanwhile, scatter diagrams were constructed using ANDVI/ANPP and FGY, and fitting was performed using linear, power, and exponential functions to construct remote sensing estimation models for FGY. In addition, measured ground samples were adopted for precision verification and evaluation, as detailed in Figure 2, Figure 3 and Table 1.

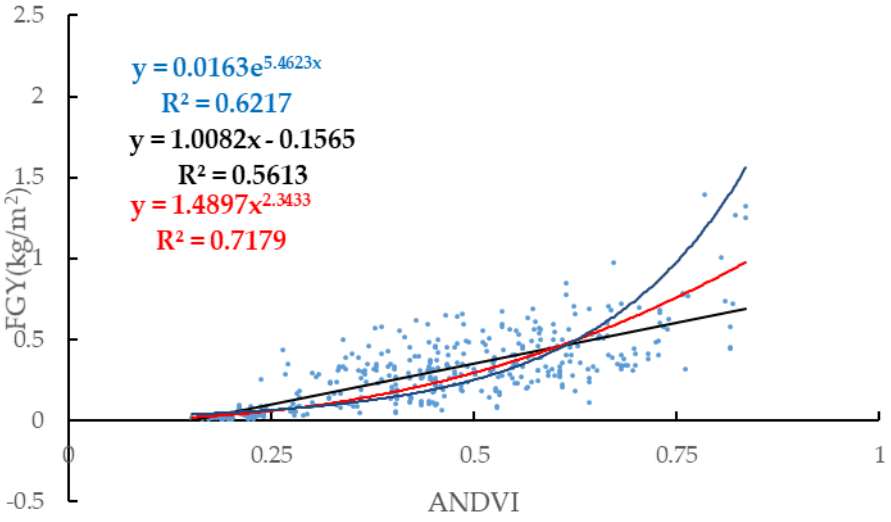

Figure 2. Scatter diagrams constructed using ANDVI and FGY.

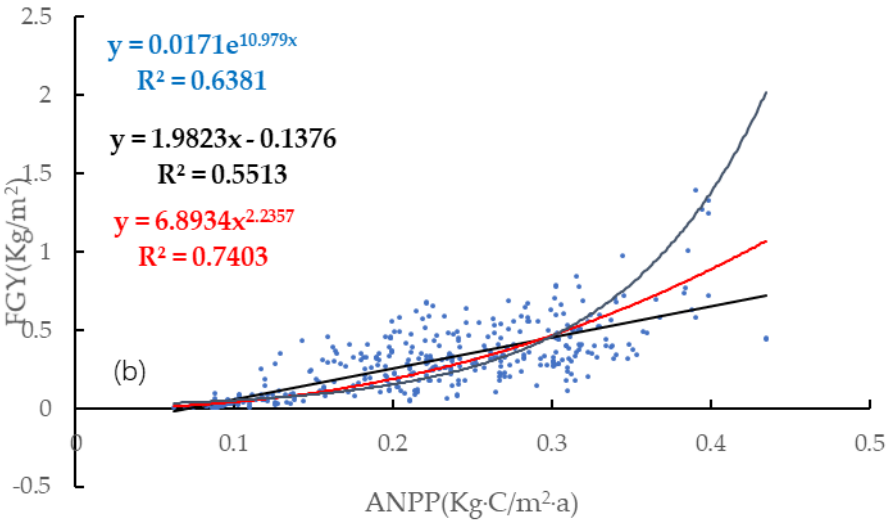

Figure 3. Scatter diagrams constructed using ANPP and FGY.

Table 1. Comparison of FGY estimation models based on ANDVI and ANPP.

Estimate main factors	Function	Formula	R^2	REE
ANDVI	linear function	$y = 1.0082x - 0.1565$	0.56	42.52%
	exponential function	$y = 0.0163e^{5.4623x}$	0.62	55.94%
ANPP	linear function	$y = 1.0082x - 0.1565$	0.56	42.52%
	linear function	$y = 1.9823x - 0.1376$	0.55	39.11%
	exponential function	$y = 0.0171e^{10.979x}$	0.64	44.76%
	power function	$y = 6.8934x^{2.2357}$	0.74	36.67%

Compared with the three fitting functions based on ANDVI, all of the three fitting functions based on ANPP, except for the linear function, had a greater R^2 value. When measured ground samples were used for testing, it was found that, regardless of the specific function used for fitting the estimation model, the precision of ANPP-based estimation models was uniformly superior to that of ANDVI-based estimation models. Thus, adopting ANPP as the main estimation factor of FGY has clear advantages. Meanwhile, through comparing the models constructed using the three functions, it was found that the exponential function had the least desirable effect, so subsequently it would not be used for fitted regression.

5.2 SST-based FGY estimation model

The above results indicated that there was a high correlation between AFY500 and ANPP, which agreed with a mathematic function (Formula (9)). In combination with Formula (6), it can be held that, theoretically, there is a high correlation between $AFY \times AVC$ and $ANPP \times RAVC$.

To verify the above assumptions and deductions, this paper constructed scatter diagrams with $AFY \times AVC$ and $ANPP \times RAVC$, and used linear and power functions for fitted regression, as shown in Figure 4. Clearly, regardless of the linear or power function used, R^2 always improved. However, the intercept of the linearly fitted regression model was negative, and, when the value of $ANPP \times RAVC$ was very small, it resulted in a negative estimate of FGY.

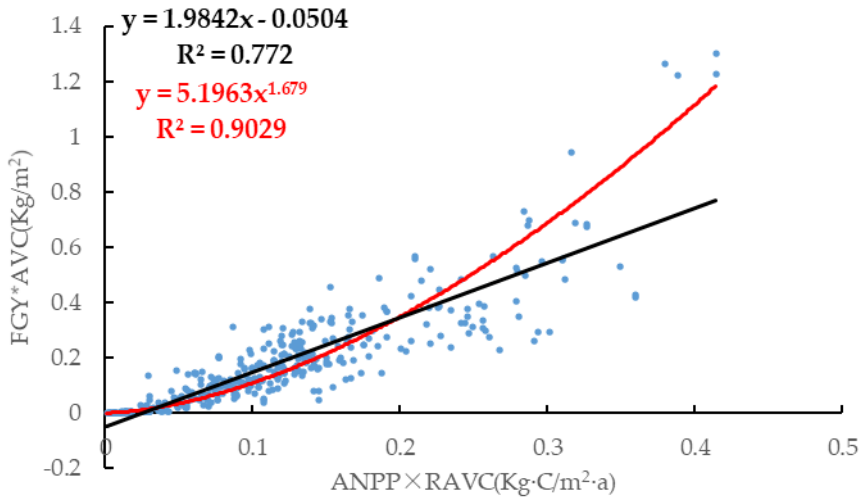

252

253 **Figure 4.** Scatter diagram constructed using AFY×AVC and ANPP×RAVC.

254 For the purpose of further improving the reliability and precision of remote sensing
255 estimation models for FGY, $ANPP_{NDVI}$ was adopted as a substitute for *ANPP*, and scatter diagrams
256 were constructed using *AFY*×*AVC* and $ANPP_{NDVI}$×*RAVC* (Figure5). As can be seen from Figure 5,
257 the correlations between the two became even more obvious (R^2_{linear}=0.81, R^2_{power}=0.93).
258 According to a comparison between Figure 4 and Figure 5, a positive intercept of the linearly
259 fitted regression model helped effectively avoid the possibility of negative grass yield when the
260 ANPP value was small. When measured ground samples data were adopted for precision
261 verification (Table 2), the REE of linear function was 18.16%, while the power function was
262 18.35%. The fitted regression models constructed using the two functions had roughly the same
263 estimation precision.

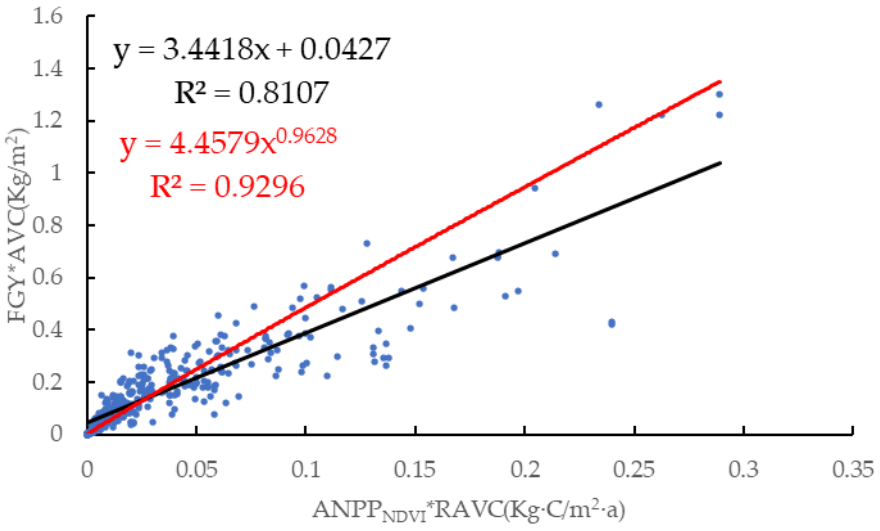

264

Figure 5. Scatter diagram constructed using $AFY \times AVC$ and $ANPP_{NDVI} \times RAVC$.

Table 2. Comparison of multi-factor composite remote sensing estimation models for grass yield.

Function	Formula	R^2	REE
Linear function	$y = 3.4418x + 0.0427$	0.81	18.16%
Power function	$y = 4.4579x^{0.9628}$	0.93	18.35%

5.3 Estimation of the grass yield of the study area

The SST-based fitted regression formulae constructed using linear and power functions were employed to estimate the grass yield for the study area, as shown in Figure 6 and Figure 7. According to the statistical results, when the fitted regression models constructed using linear and power functions were used to estimate the total FGY of the grassland in the study area, the respective results were 8.777×10^{10} kg and 8.583×10^{10} kg, so there was no significant gap. Relative to the power function fitted model, the linear function fitted model had a relative precision of 97.8%; relative to the linear function fitted model, the power function fitted model had a relative precision of 97.7%.

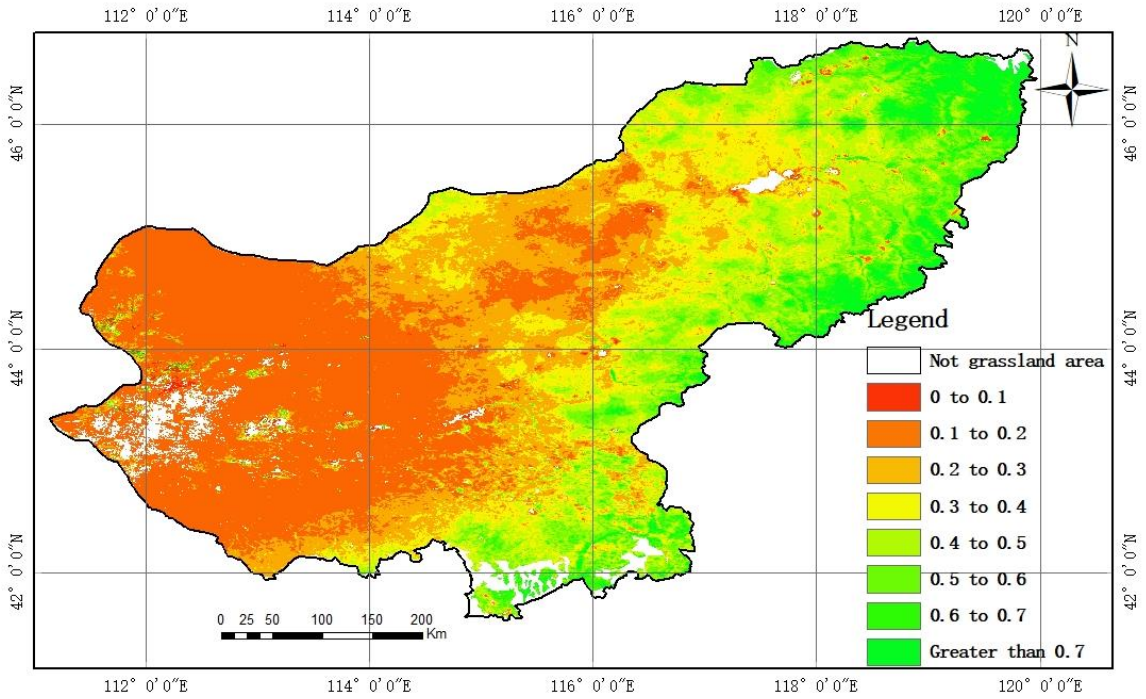

Figure 6. Results estimated by the linear function fitted model.

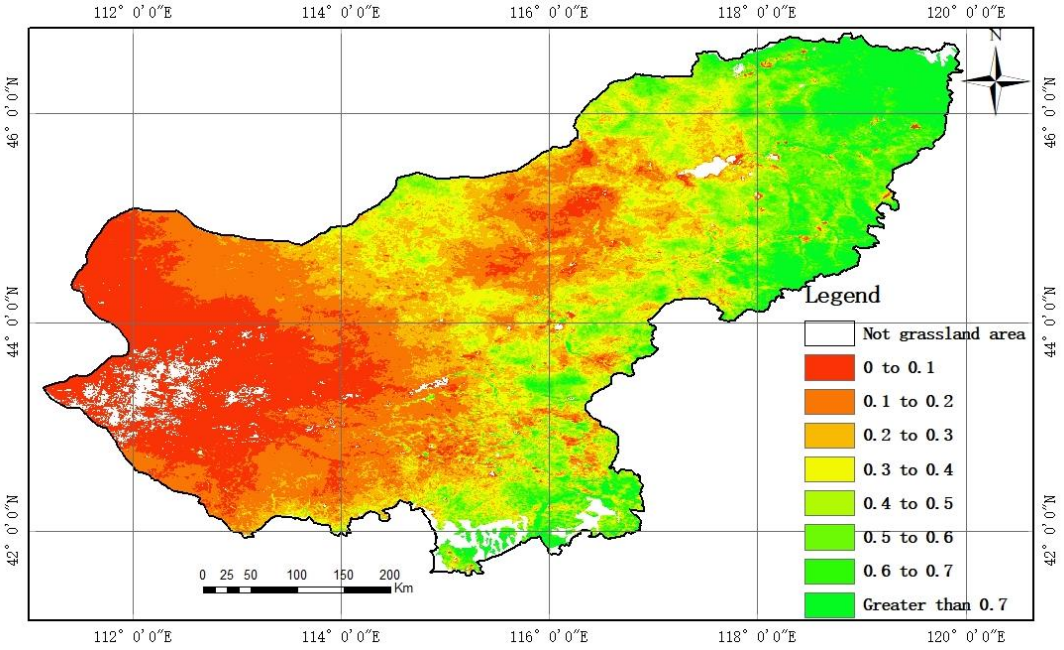

Figure 7. Results estimated by the power function fitted model.

A comparison between Figure 6 and Figure 7 revealed that, spatially, the two models had similar overall trends for FGY per unit; however, significant differences in spatial distribution could be observed. As indicated by the statistical results (Table 3), in the west and middle of the study area, the area with a FGY per unit of less than 0.1 kg/m^2 estimated by the power function fitted model was far greater than that estimated by the linear function fitted model. In the east and south of the study area, the area with a FGY per unit of greater than 0.7 kg/m^2 estimated by the power function fitted model was also far greater than that estimated by the linear function fitted model. However, due to the lack of data on large-scale regional FGY, it was difficult to evaluate the advantages and disadvantages of the two models. In follow-up research, the coverage of ground samples will be expanded to further explore this issue.

Table 3. Statistics on grass yield per unit.

FGY per unit (kg/m^2)	Linear function model	Power function model
less than 0.1	0.12%	18.95%
0.1-0.2	33.68%	20.29%
0.2-0.3	18.97%	16.09%
0.3-0.4	14.93%	13.82%
0.4-0.5	13.80%	9.83%
0.5-0.6	9.29%	7.58%
0.6-0.7	4.68%	5.11%
greater than 0.7	4.54%	8.34%

6 Conclusion

The global NPP product provided by MODIS tended to compromise grass yield estimation precision due to the uncertainty of self-inversion. However, as indicated by a comparison between remote sensing estimation models adopting NPP and NDVI as the main estimation factor for FGY, NPP produced more desirable results. Given the failure to improve estimation precision due to the inconsistency between remote sensing data and ground samples on spatial scales, SST was performed using the vegetation coverage before and after modification, and a SST-based FGY estimation model was proposed. As demonstrated by the results of the case study based on the grassland in Xilingol League, the model effectively improved estimation precision.

The SST-based fitted regression models constructed using linear and power functions were employed to estimate the total FGY for the entire study area, resulting in respective estimates of 8.777×10^{10} kg and 8.583×10^{10} kg. Therefore, the two models obtained roughly the same estimate, and their spatial distribution trends were also consistent. However, there were significant differences in the spatial distribution of FGY per unit, which calls for follow-up research. Based on this comprehensive analysis, the research group draws the conclusion that when using the MODIS-NPP data product as the main variable, the SST-based FGY estimation model can be used to estimate regional grass yield.

Acknowledgments

This research was partially supported by Natural Science Foundation of China (No. 42071246) and Natural Fund Commission of Hebei Province (No. E2020402006).

References

Bella, D. et al., 2004. Remote sensing capabilities to estimate pasture production in France. International Journal of Remote Sensing, 25(23): 5359-5372.

Feng, X.M. and Zhao, Y.S., 2011. Grazing intensity monitoring in Northern China steppe: Integrating CENTURY model and MODIS data. Ecological Indicators, 11(1): 175-182.

Fry, E.L. et al., 2013. Plant functional group composition modifies the effects of precipitation change on grassland ecosystem function. PloS one, 8(2).

Fu, X., Tang, C., Zhang, X., Fu, J. and Jiang, D., 2014. An improved indicator of simulated grassland production based on MODIS NDVI and GPP data: A case study in the Sichuan province, China. Ecological Indicators, 40: 102-108.

Gao, H., Pan, X.B. and Fu, Y., 2009. Influence of climate change on potential climate productivity in grassland of central Inner Mongolia. Chinese Journal of Agrometeorology, 30(3): 277-282.

Gao, T. et al., 2013. Spatio-temporal variation in vegetation biomass and its relationships with climate factors in the Xilingol grasslands, Northern China. PLoS One, 8(12).

Gao, T. et al., 2013. Using MODIS time series data to estimate aboveground biomass and its spatio-temporal variation in Inner Mongolia's grassland between 2001 and 2011. International Journal of Remote Sensing, 34(21): 7796-7810.

Ge, J. et al., 2018. Modeling alpine grassland cover based on MODIS data and support vector machine regression in the headwater region of the Huanghe River, China. Remote sensing of environment, 218: 162-173.

Gitelson, A.A. et al., 2012. Remote estimation of crop gross primary production with Landsat data. Remote Sensing of Environment, 121: 404-414.

Goetz, S.J., Prince, S.D., Goward, S.N., Thawley, M.M. and Small, J., 1999. Satellite remote sensing of primary production: an improved production efficiency modeling approach. Ecological Modelling, 122(3): 239-255.

Inoue, Y., Peñuelas, J., Miyata, A. and Mano, M., 2008. Normalized difference spectral indices for estimating photosynthetic efficiency and capacity at a canopy scale derived from hyperspectral and CO2 flux measurements in rice. Remote Sensing of Environment, 112(1): 156-172.

Li, G., Xin, X.P., Wang, D.L. and Shi, R.X., 2007. Application of improved CASA model in productivity evaluation of grassland in Inner Mongolia. Chinese Journal of Ecology, 26(12): 2100-2106.

Li, Z., Liu, Z. and Chen, Z., 2003. The effects of climate changes on the productivity in the Inner Mongolia steppe of China. Acta Prataculturae Sinica, 12(1): 4-10.

Liu, A.J., Wang, J.J. and Han, J.G., 2007. Study on method of estimating net primary production of rangeland by remote sensing-a case study of Xilingol grassland. Chinese Journal of Grassland, 29: 31-37.

Liu, H. et al., 2016. The Spatiotemporal Variation of Drought in the Beijing-Tianjin-Hebei Metropolitan Region (BTHMR) Based on the Modified TVDI. Sustainability, 8(12): 1327.

Liu, J. et al., 2020. Modeling grass yields in Qinghai Province, China, based on MODIS NDVI data—an empirical

348 comparison. Frontiers of Earth Science: 1-17.
349 Luo, G. et al., 2012. Moderate grazing can promote aboveground primary production of grassland under water
350 stress. Ecological Complexity, 11: 126-136.
351 Matsushita, B. and Tamura, M., 2002. Integrating remotely sensed data with an ecosystem model to estimate net
352 primary productivity in East Asia. Remote Sensing of Environment, 81(1): 58-66.
353 Ni, J., 2004. Estimating net primary productivity of grasslands from field biomass measurements in temperate
354 northern China. Plant Ecology, 174(2): 217-234.
355 Suttie, J.M., Reynolds, S.G. and Batello, C., 2005. Grasslands of the World, 34. Food & Agriculture Org.
356 Viña, A. and Gitelson, A.A., 2005. New developments in the remote estimation of the fraction of absorbed
357 photosynthetically active radiation in crops. Geophysical Research Letters, 32(17).
358 Wu, C., Han, X., Ni, J., Niu, Z. and Huang, W., 2010. Estimation of gross primary production in wheat from in
359 situ measurements. International Journal of Applied Earth Observation and Geoinformation, 12(3): 183-189.
360 Xie, G., Zhang, Y., Lu, C., Zheng, D. and Cheng, S., 2001. Study on valuation of rangeland ecosystem services of
361 China. Journal of Natural Resources, 16(1): 47-53.
362 Xu, B. et al., 2007. Remote sensing monitoring upon the grass production in China. Acta Ecologica Sinica, 27(2):
363 405-413.
364 Xu, B. et al., 2008. MODIS-based remote sensing monitoring of grass production in China. International Journal
365 of Remote Sensing, 29(17-18): 5313-5327.
366 Xu, B. et al., 2013. MODIS-based remote-sensing monitoring of the spatiotemporal patterns of China's grassland
367 vegetation growth. International journal of remote sensing, 34(11): 3867-3878.
368 Xu, B. and Yang, X., 2009. Calculation of grass production and balance of livestock carrying capacity in rangeland
369 region of Northeast China. Geographical Research, 28(2): 402-408.
370 Yang, X., Xu, B., Zhu, X., Tao, W. and Liu, T., 2007. Models of grass production based on remote sensing
371 monitoring in northern agro-grazing ecotone [J]. Geographical Research, 2.
372 Yang, Y.H., Fang, J.Y., Pan, Y.D. and Ji, C.J., 2009. Aboveground biomass in Tibetan grasslands. Journal of Arid
373 Environments, 73(1): 91-95.
374 Yang, Z.L., Du, W.X., Hou, Q., Li, X. and Wang, B., 2008. Regional analysis of climate change in the east of
375 Inner Mongolia and its potential productivity of grassland. Chin. J. Grassl, 30: 62-66.

Zhang, F., Zhou, G.S. and Wang, Y.H., 2008. Dynamics simulation of net primary productivity by a satellite data-driven CASA model in Inner Mongolian typical steppe. China. J. Plant Ecol, 32(4): 786-797.

Zhao, F. et al., 2014. Remote Sensing Estimates of Grassland Aboveground Biomass Based on MODIS Net Primary Productivity (NPP): A Case Study in the Xilingol Grassland of Northern China. Remote Sensing, 6(6): 5368-5386.

Zhou, W., Li, J. and Yue, T., 2020. The Variation of Landscape and NPP of Main Pastoral Grasslands in China. Springer, pp. 83-104.

Zribi, M. et al., 2003. Derivation of wild vegetation cover density in semi-arid regions: ERS2/SAR evaluation. International Journal of Remote Sensing, 24(6): 1335-1352.

Table captions

394
395 **Table 1.** Comparison of FGY estimation models based on ANDVI and ANPP.

Estimate main factors	Function	Formula	R^2	REE
ANDVI	linear function	$y = 1.0082x - 0.1565$	0.56	42.52%
	exponential function	$y = 0.0163e^{5.4623x}$	0.62	55.94%
	linear function	$y = 1.0082x - 0.1565$	0.56	42.52%
ANPP	linear function	$y = 1.9823x - 0.1376$	0.55	39.11%
	exponential function	$y = 0.0171e^{10.979x}$	0.64	44.76%
	power function	$y = 6.8934x^{2.2357}$	0.74	36.67%

396
397

398
399 **Table 2.** Comparison of multi-factor composite remote sensing estimation models for grass yield.

Function	Formula	R^2	REE
Linear function	$y = 3.4418x + 0.0427$	0.81	18.16%
Power function	$y = 4.4579x^{0.9628}$	0.93	18.35%

400
401

402
403

Table 3. Statistics on grass yield per unit.

FGY per unit (kg/m²)	**Linear function model**	**Power function model**
less than 0.1	0.12%	18.95%
0.1-0.2	33.68%	20.29%
0.2-0.3	18.97%	16.09%
0.3-0.4	14.93%	13.82%
0.4-0.5	13.80%	9.83%
0.5-0.6	9.29%	7.58%
0.6-0.7	4.68%	5.11%
greater than 0.7	4.54%	8.34%

404
405

Figure captions

Figure 1. Grassland types and sampling points in the study area.

Figure 2. Scatter diagrams constructed using ANDVI and FGY.

Figure 3. Scatter diagrams constructed using ANPP and FGY.

Figure 4. Scatter diagram constructed using $AFY \times AVC$ and $ANPP \times RAVC$.

Figure 5. Scatter diagram constructed using $AFY \times AVC$ and $ANPP_{NDVI} \times RAVC$.

Figure 6. Results estimated by the linear function fitted model.

Figure 7. Results estimated by the power function fitted model.

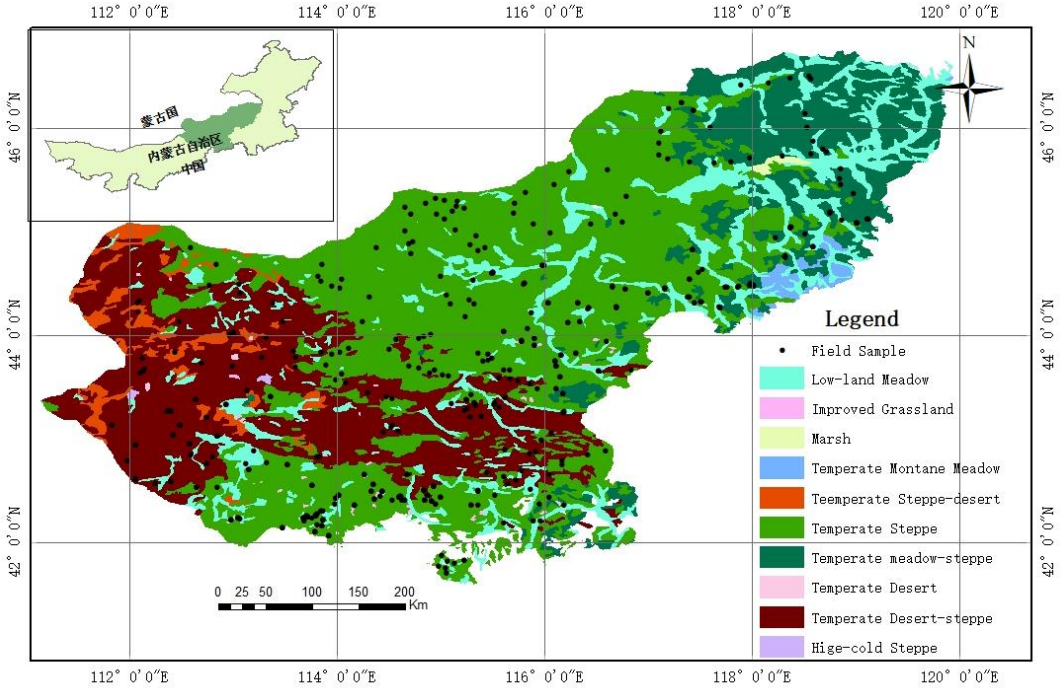

Figure 1. Grassland types and sampling points in the study area.

420

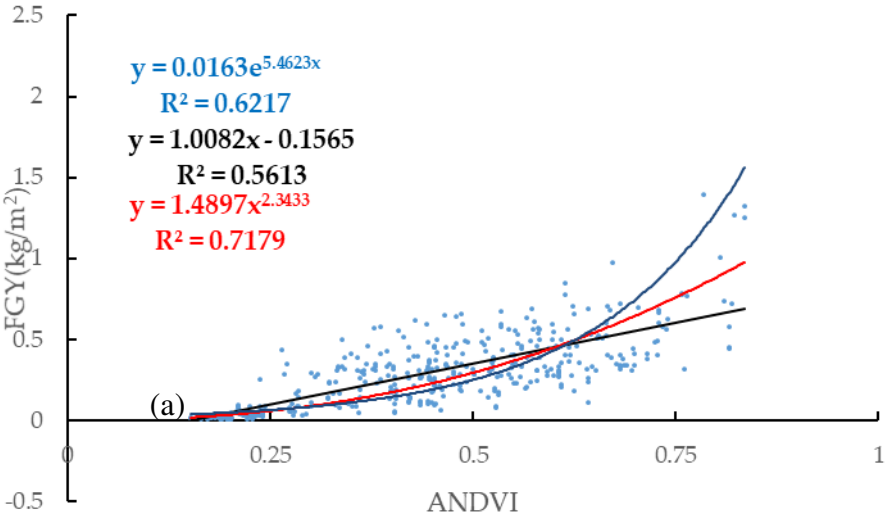

421

422 **Figure 2.** Scatter diagrams constructed using ANDVI and FGY.

423

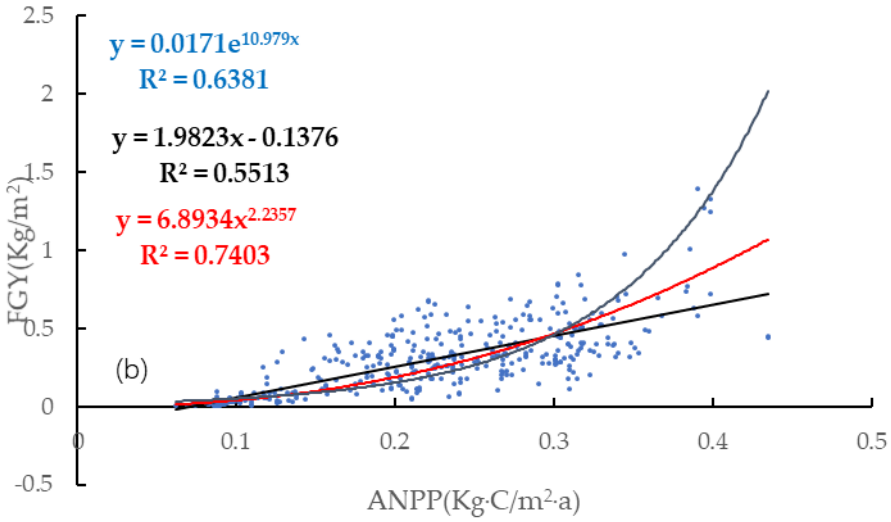

Figure 3. Scatter diagrams constructed using ANPP and FGY.

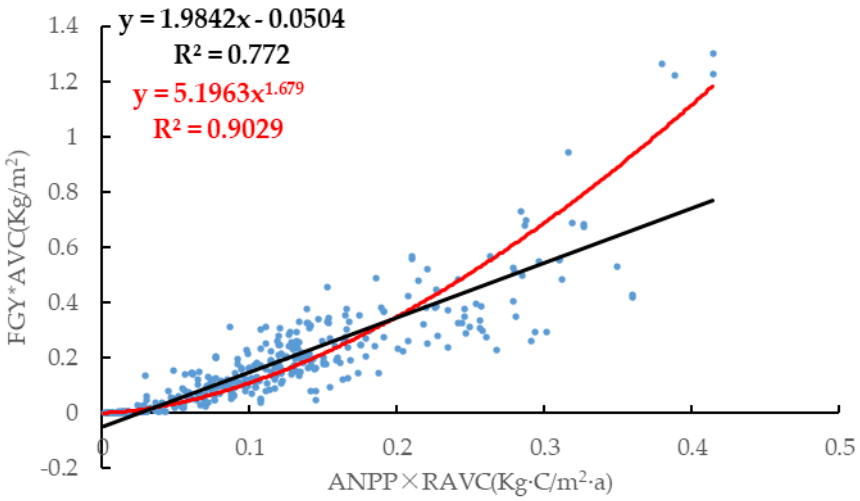

Figure 4. Scatter diagram constructed using *AFY×AVC* and *ANPP×RAVC*.

433

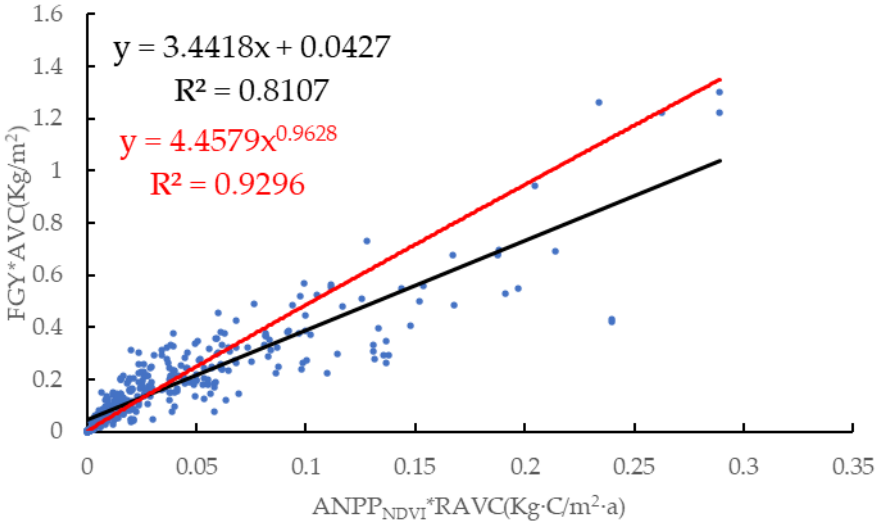

434

435 **Figure 5.** Scatter diagram constructed using *AFY*×*AVC* and *ANPP*$_{NDVI}$×*RAVC*.

436

437

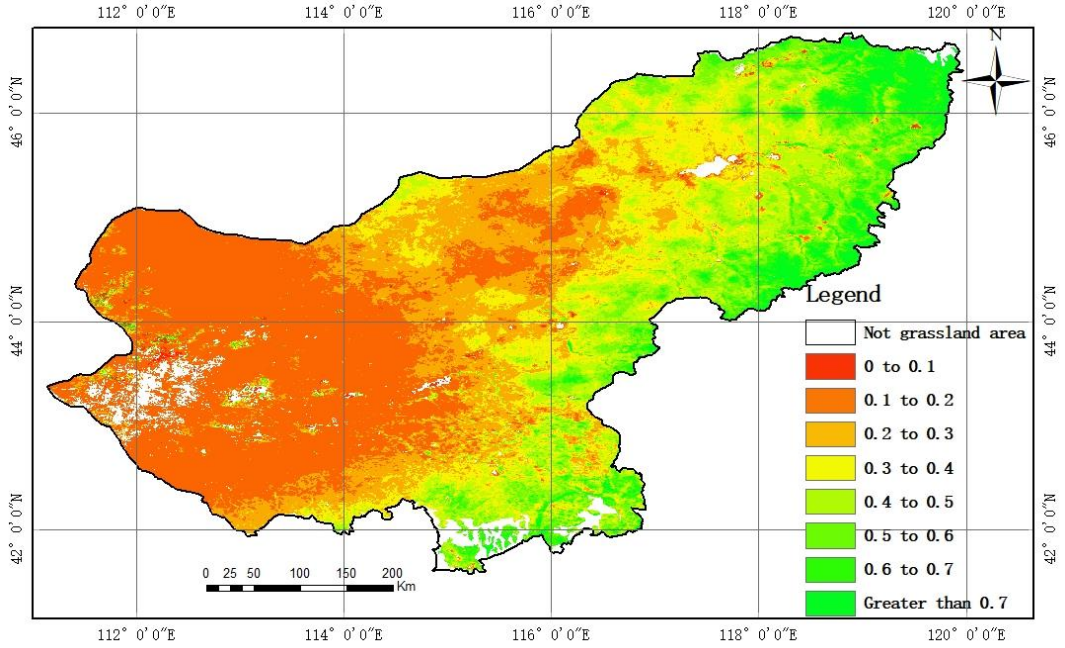

438

439 **Figure 6.** Results estimated by the linear function fitted model.

440

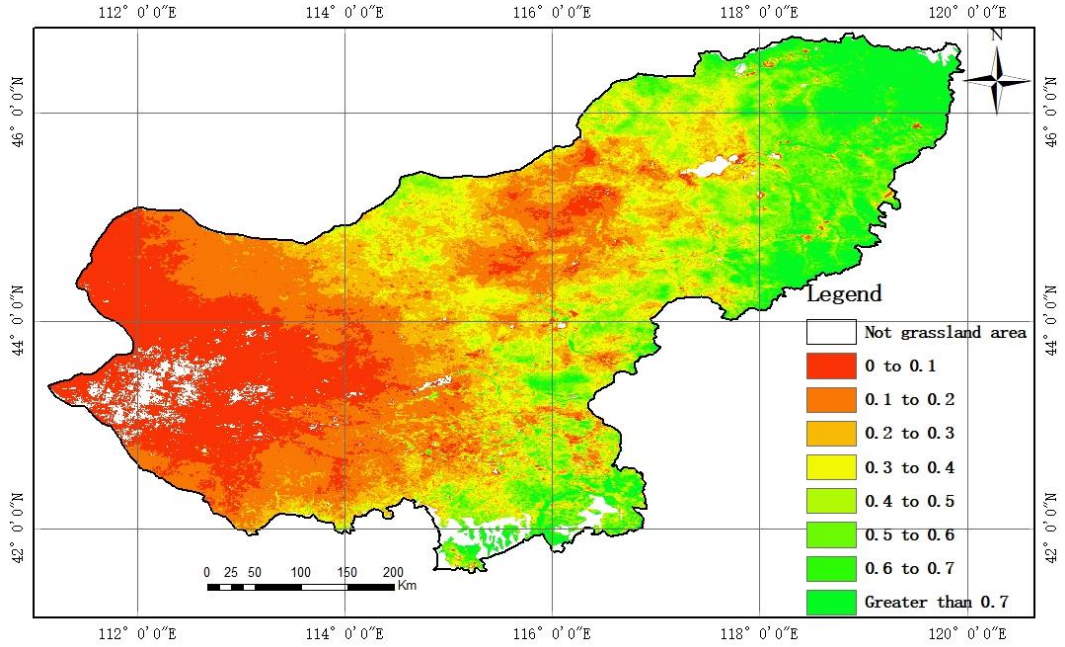

Figure 7. Results estimated by the power function fitted model.

Figures

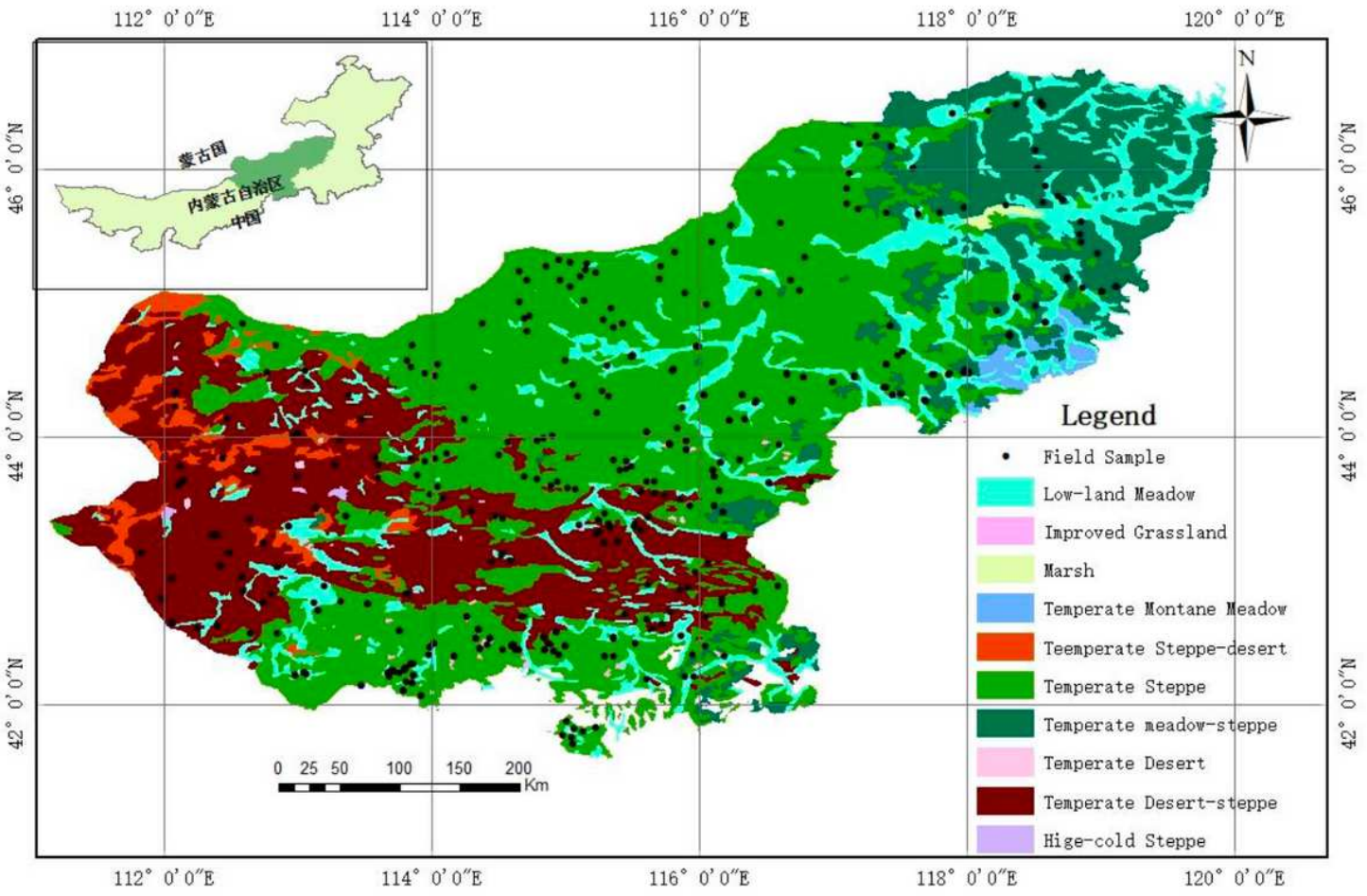

Figure 1

Grassland types and sampling points in the study area. Note: The designations employed and the presentation of the material on this map do not imply the expression of any opinion whatsoever on the part of Research Square concerning the legal status of any country, territory, city or area or of its authorities, or concerning the delimitation of its frontiers or boundaries. This map has been provided by the authors.

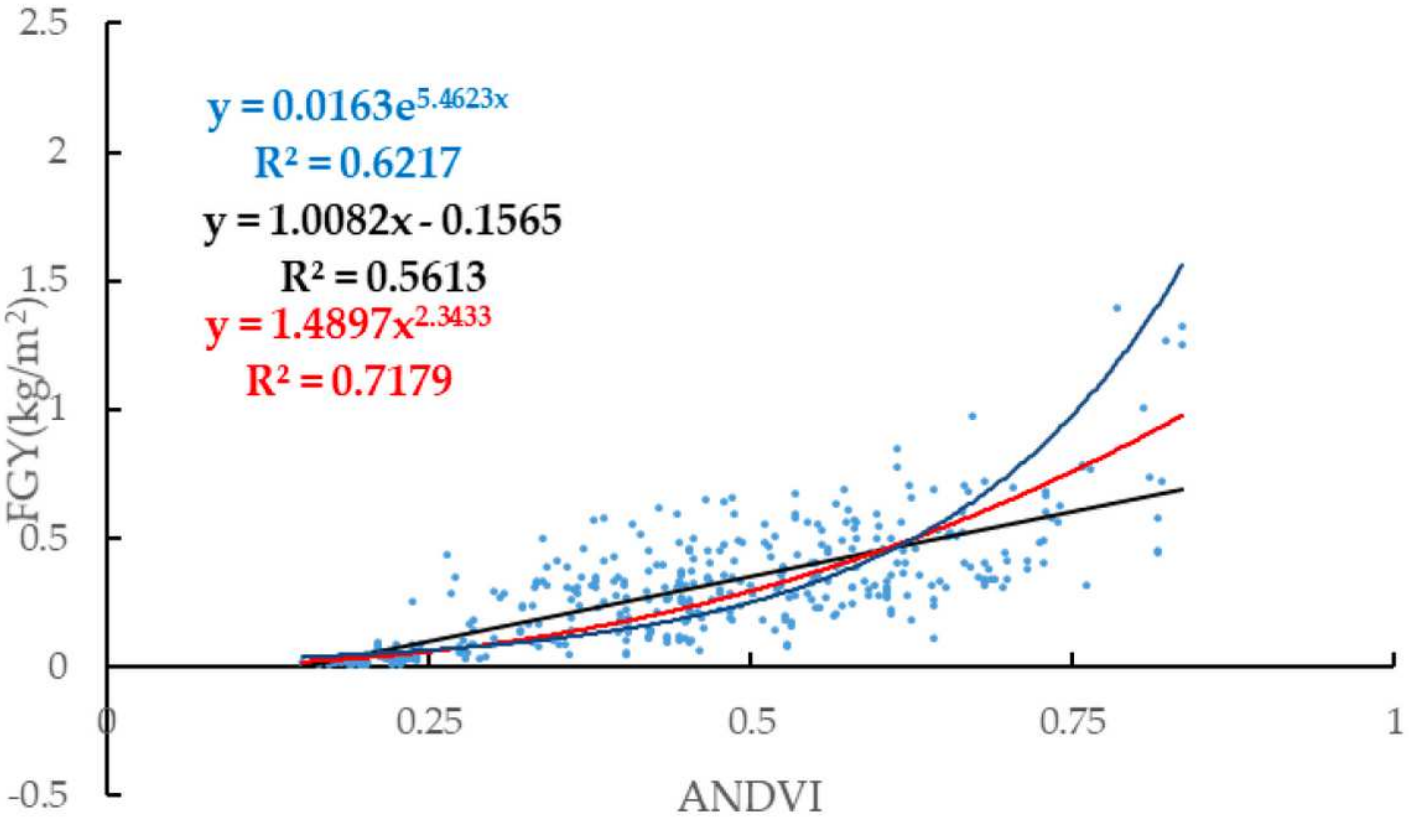

Figure 2

Scatter diagrams constructed using ANDVI and FGY.

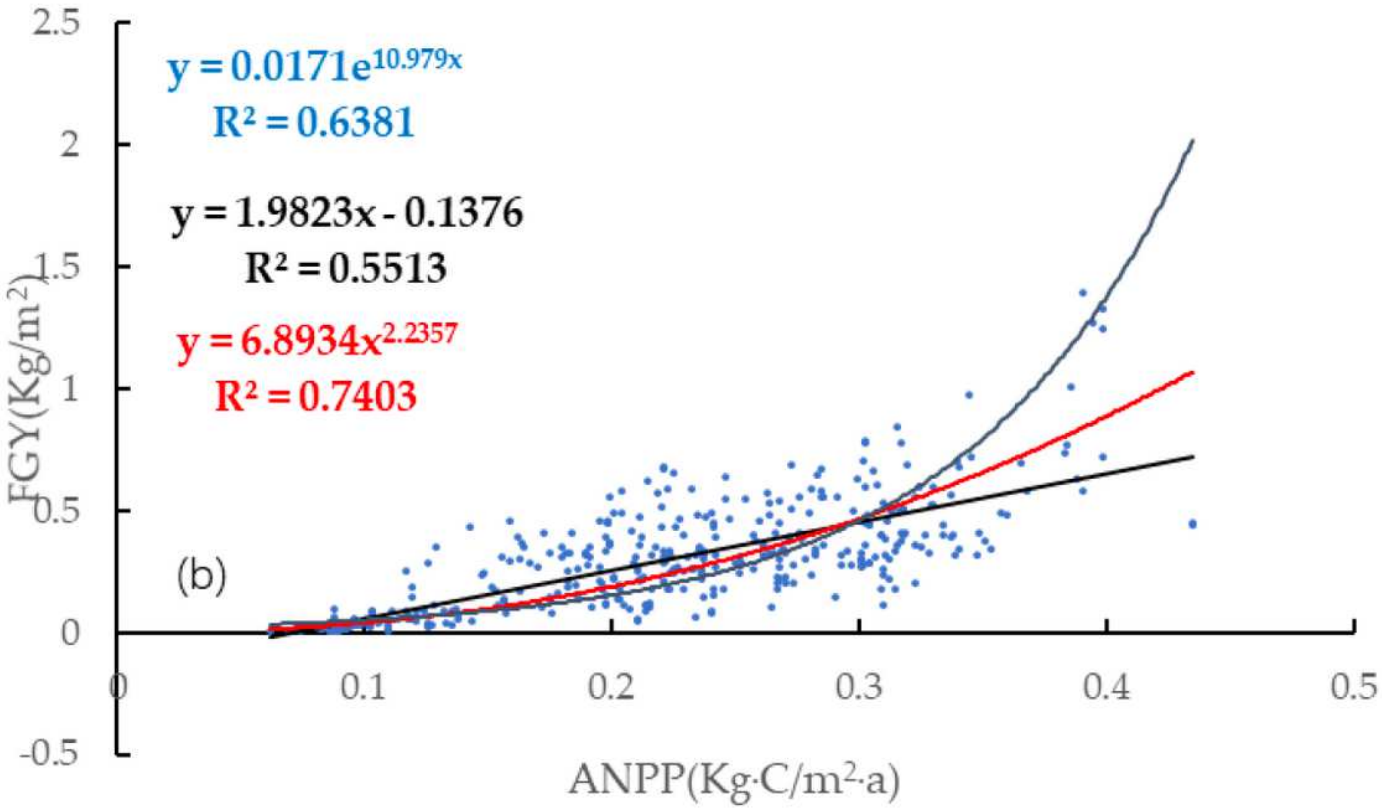

Figure 3

Scatter diagrams constructed using ANPP and FGY.

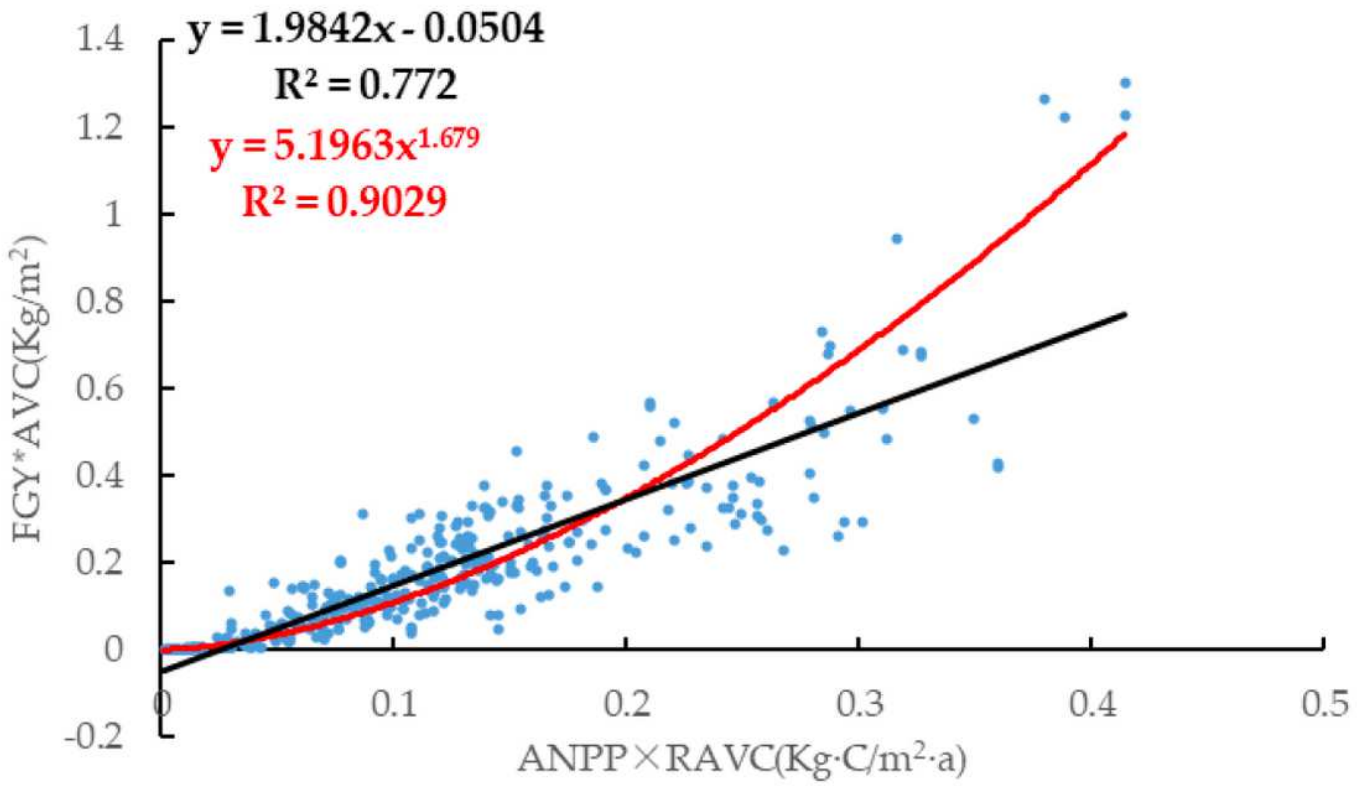

Figure 4

Scatter diagram constructed using AFY×AVC and ANPP×RAVC.

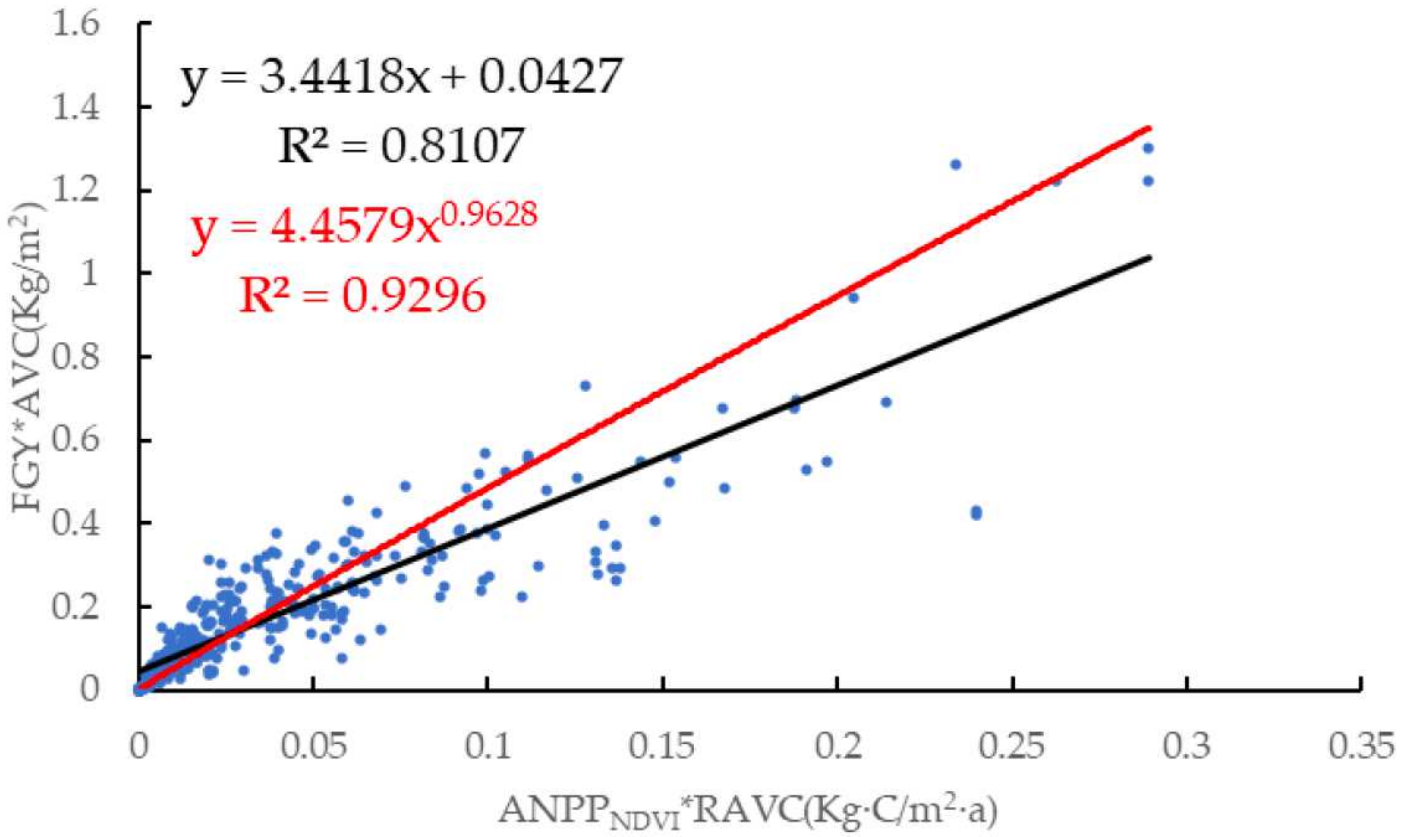

Figure 5

Scatter diagram constructed using AFY×AVC and ANPPNDVI×RAVC.

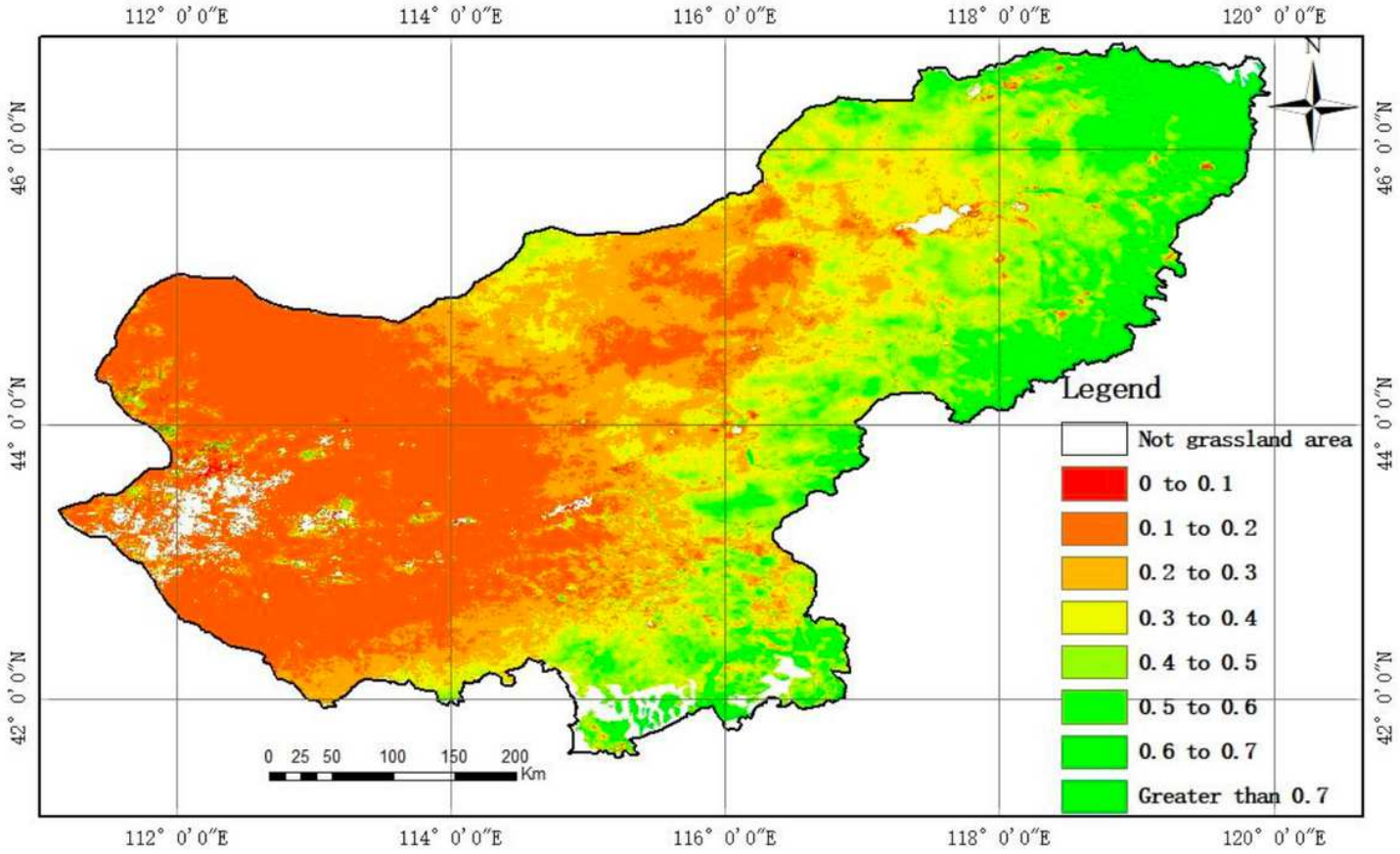

Figure 6

Results estimated by the linear function fitted model. Note: The designations employed and the presentation of the material on this map do not imply the expression of any opinion whatsoever on the part of Research Square concerning the legal status of any country, territory, city or area or of its authorities, or concerning the delimitation of its frontiers or boundaries. This map has been provided by the authors.

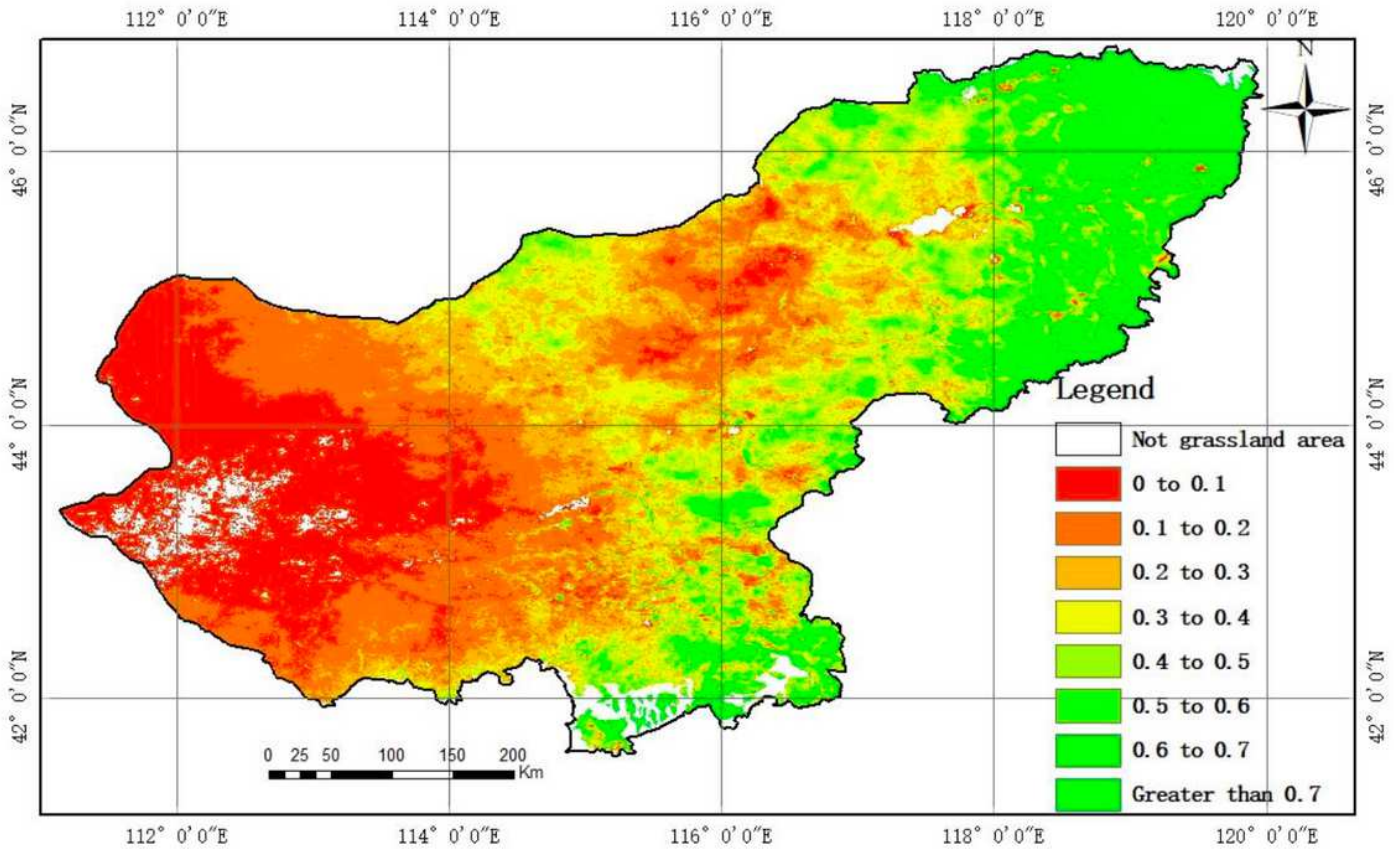

Figure 7

Results estimated by the power function fitted model. Note: The designations employed and the presentation of the material on this map do not imply the expression of any opinion whatsoever on the part of Research Square concerning the legal status of any country, territory, city or area or of its authorities, or concerning the delimitation of its frontiers or boundaries. This map has been provided by the authors.